

Cite this: *J. Mater. Chem. B*,
2024, 12, 6146

Supramolecular assembly of isomeric SN-38 prodrugs regulated by conjugation sites†

Zhenhai Tang, Jianhua Zhang, Wenting Li, Kaiying Wen, Zhipeng Gu, 
Dongdong Zhou * and Hao Su *

Supramolecular polymers (SPs) are an emerging class of drug transporters employed to improve drug therapy. Through the rational design of self-assembling monomers, one can optimize the properties of the resulting supramolecular nanostructures, such as size, shape, surface chemistry, release, and, therefore, biological fates. This study highlights the design of isomeric SN38 prodrugs through the conjugation of hydrophilic oligo(ethylene glycol) (OEG) with hydroxyls at positions 10 and 20 on hydrophobic SN-38. Self-assembling prodrug (SAPD) isomers 10-OEG-SN38 and 20-OEG-SN38 can self-assemble into giant nanotubes and filamentous assemblies, respectively, *via* aromatic associations that dominate self-assembly. Our study reveals the influence of modification sites on the assembly behavior and ability of the SN38 SAPDs, as well as drug release and subsequent *in vitro* and *in vivo* antitumor effects. The SAPD modified at position 20 exhibits stronger π - π interactions among SN38 units, leading to more compact packing and enhanced assembly capability, whereas OEG at position 10 poses steric hindrance for aromatic associations. Importantly, owing to its higher chemical and supramolecular stability, 20-OEG-SN38 outperforms 10-OEG-SN38 and irinotecan, a clinically used prodrug of SN38, in a CT26 tumor model, demonstrating enhanced tumor growth inhibition and prolonged animal survival. This study presents a new strategy of using interactions among drug molecules as dominating features to create supramolecular assemblies. It also brings some insights into creating effective supramolecular drug assemblies *via* the engineering of self-assembling building blocks, which could contribute to the optimization of design principles for supramolecular drug delivery systems.

Received 3rd April 2024,
Accepted 20th May 2024

DOI: 10.1039/d4tb00717d

rsc.li/materials-b

Introduction

Supramolecular polymers (SPs) constructed *via* the non-covalent linkage of monomeric units offer great advantages in improving the delivery of drugs.^{1–3} One unique feature is that the physicochemical properties of supramolecular nanostructures can be facily controlled *via* the molecular-level design of self-assembling building blocks. For example, the morphologies of peptide assemblies are highly sequence-specific^{4–6} and sensitive to the amino acid position in isomeric peptide sequences.^{7–9} In other examples, the self-assembly behavior of monomeric building blocks is controlled by the attachment and removal of enzyme cleavable pendant functional groups, enabling the sol-gel transition of supramolecular materials.^{10,11} In addition, the composition and functionality of SPs can be tuned *via* the supramolecular copolymerization of

multiple monomers.^{12,13} Among these monomeric units, self-assembling prodrugs (SAPDs) have been recently recognized as a class of novel monomers of particular interest that are capable of spontaneously associating into SPs in aqueous solutions, achieving self-formulation and self-delivery of active drugs.^{14,15} Conjugation of hydrophobic drugs to hydrophilic auxiliaries affords amphiphilic prodrugs, which subsequently self-assemble into discrete drug nanostructures in aqueous environments. Compared with traditional nanomedicines prepared *via* drug encapsulation, this strategy avoids external carriers, which could potentially overcome the heterogeneity between drug molecules and carriers, thereby significantly increasing drug loading and reducing the toxicity risk from drug leakage and external carrier materials. The physicochemical properties, such as size, shape, surface chemistry, internal ordering, and stability, of the resulting drug assemblies can be meticulously regulated through the design and refinement of the prodrug molecular structure, thereby offering high levels of operability.^{16,17} For example, block copolymer-drug conjugates consisting of poly(ethylene glycol)-poly(α,β -aspartic acid) (PEG-*b*-PAsp) and doxorubicin can assemble into drug-containing micelles.¹⁸ The Chikoti group synthesized a class of chimeric

College of Polymer Science and Engineering, State Key Laboratory of Polymer Materials Engineering, Sichuan University, Chengdu 610065, China.

E-mail: hsu@scu.edu.cn, zhoud@scu.edu.cn

† Electronic supplementary information (ESI) available. See DOI: <https://doi.org/10.1039/d4tb00717d>

This tendency leads to more compact packing and enhanced assembly capabilities. Conversely, the chiral stacking of SN38 is disrupted when modification occurs at the 10-site, resulting in compromised assembly capacity. These disparities directly affect the drug release, cytotoxicity and therapeutic efficacy of the SAPDs both *in vitro* and *in vivo*. Our results provide an example of using interactions among drug molecules as dominating features to create supramolecular assemblies and the strategic selection of the most appropriate hydroxyl modification sites for designing SN38 SAPD to maximize its performance in self-assembly and therapy.

Experimental section

1 Synthesis of OEG-NO₂

Pentaethylene glycol monomethyl ether (OEG₅-OH, 1.00 g, 3.9 mmol), 4-dimethylamino pyridine (DMAP, 1.65 g, 13.5 mmol) and 4-nitrobenzoyl chloride were mixed together into dry DCM (30 ml) and then stirred at room temperature overnight. The reaction mixture was evaporated to remove the solvent, and the residue was further purified by chromatography on silica gel with EA/PE (1/9 to 1/1) and then EA/MeOH (19/1) as the eluent to obtain the OEG-NO₂ (colorless oil, 1.2 g, 73%). ¹H NMR (300 MHz; CDCl₃; ppm): δ 3.38 (s, 3H), 3.50–3.85 (m, 18H), 4.40–4.47 (m, 2H), 7.34–7.46 (m, 2H), 8.22–8.34 (m, 2H). MS (ESI-MS) *m/z*: [M + H]⁺ calculated for C₁₈H₂₇NO₁₀, 418.16; found, 418.05.

2 Synthesis of 10-OEG-SN38

SN38 (0.34 g, 0.86 mmol) was suspended in a DCM solution (20 ml) of OEG-NO₂ (0.3 g, 0.72 mmol) and triethylamine (0.36 g, 3.59 mmol). The reaction mixture was stirred for 24 hours. After removing the solvent under a vacuum, the residue was first purified by flash chromatography on silica gel with DCM/MeOH (10/1) and then by RP-HPLC (10-SN38-OEG, white solid, 0.3 g, 62%). ¹H NMR (300 MHz; CDCl₃; ppm): δ 1.0–1.08 (t, 3H), 1.36–1.44 (s, 3H), 1.81–1.98 (m, 2H), 3.10–3.22 (q, 2H), 3.34–3.41 (s, 3H), 3.49–3.91 (m, 20H), 4.44–4.51 (m, 2H), 5.22–5.36 (m, 3H), 5.71–5.80 (d, 1H), 7.61–7.70 (t, 2H), 7.90–7.96 (s, 1H), 8.21–8.29 (d, 1H). MS (ESI-MS) *m/z*: [M + H]⁺ calculated for C₃₄H₄₂N₂O₁₂, 670.27; found, 671.12.

3 Synthesis of 20-OEG-SN38

SN38 (1 g, 2.55 mmol) was suspended in a solution of di-*tert*-butyl dicarbonate (0.72 g, 3.3 mmol) and triethylamine (0.52 g, 5 mmol) in DCM (40 ml). After being stirred at room temperature for 48 h, the resulting mixture was washed three times with 0.5 M HCl (40 ml) and brine (40 ml) and then dried using anhydrous sodium sulfate to obtain 10-BOC-SN38 (pale-yellow solid, 1.02 g, 92%). ¹H NMR (300 MHz; CDCl₃; ppm): δ 0.97–1.10 (t, 3H), 1.34–1.46 (s, 3H), 1.52–1.68 (s, 9H), 1.81–1.99 (m, 2H), 3.08–3.24 (q, 2H), 5.21–5.37 (m, 3H), 5.68–5.82 (d, 1H), 7.59–7.72 (t, 2H), 7.85–7.94 (s, 1H), 8.19–8.27 (d, 1H).

10-BOC-SN38 (0.4 g, 0.9 mmol), OEG-NO₂ (0.46 g, 1 mmol) and DMAP (0.25 g, 2 mmol) were dissolved in DCM (30 ml). The reaction mixture was heated reflux at 55 °C and stirred

overnight. The yellow solution was concentrated *in vacuo*, and the residue was further purified using RP-HPLC. The product fractions were combined and lyophilized to give 10-Boc-20-OEG-SN38 (pale-yellow solid, 0.3 g, 43%). ¹H NMR (300 MHz; CDCl₃; ppm): δ 0.95–1.04 (t, 3H), 1.35–1.43 (s, 3H), 1.61–1.64 (s, 9H), 2.08–2.34 (m, 2H), 3.12–3.21 (q, 2H), 3.35–3.40 (s, 3H), 3.5–3.75 (m, 17H), 4.19–4.32 (m, 2H), 5.22–5.30 (s, 2H), 5.35–5.74 (q, 2H), 7.28–7.33 (s, 1H), 7.64–7.72 (d, 1H), 7.88–7.93 (s, 1H), 8.20–8.26 (d, 1H).

Trifluoroacetic acid (TFA, 0.88 g, 7.8 mmol) was added dropwise to a solution of 10-Boc-20-OEG-SN38 (0.3 g, 0.39 mmol) in DCM (10 ml). The resulting mixture was washed with a saturated solution of NaHCO₃ and dried over anhydrous sodium sulfate. The mixture was concentrated *in vacuo* to obtain the 20-OEG-SN38 (bright yellow powder, 0.22 g, 84.6%). ¹H NMR (300 MHz; CDCl₃; ppm): δ 1.01–1.05 (t, 3H), 1.25–1.38 (s, 3H), 2.10–2.30 (m, 2H), 2.96–3.10 (q, 2H), 3.35–3.45 (s, 3H), 3.46–3.78 (m, 19H), 4.13–4.33 (m, 2H), 5.02–5.18 (s, 2H), 5.32–5.77 (q, 2H), 7.28–7.30 (s, 1H), 7.31–7.38 (s, 1H), 7.44–7.55 (d, 1H), 8.01–8.12 (d, 1H). MS (ESI-MS) *m/z*: [M + H]⁺ calculated for C₃₄H₄₂N₂O₁₂, 670.27; found, 671.13.

4 Synthesis of di-OEG-SN38

SN38 (0.5 g, 1.274 mmol) was suspended in the solution of triphosgene (0.2647 g, 0.892 mmol) in dry DCM (50 ml). DMAP (0.7165 g, 5.86 mmol) was dissolved in dry DCM (20 ml) and added dropwise to the mixture. After one hour, OEG (0.7073 g, 2.80 mmol) was then added to the mixture and stirred overnight. The mixture was washed with 0.5 M HCl (50 ml × 3) and brine (50 ml × 3). Then, the extracts were dried with anhydrous sodium sulfate. The reaction mixture was concentrated under a vacuum, and the residue was purified using RP-HPLC. The product fractions were combined and lyophilized to produce di-OEG-SN38 (pale-yellow solid, 0.6 g, 50%). ¹H NMR (300 MHz; CDCl₃; ppm): δ 0.99–1.05 (t, 3H), 1.25–1.39 (s, 3H), 2.10–2.30 (m, 2H), 2.96–3.10 (q, 2H), 3.08–3.78 (m, 46H), 4.17–4.32 (m, 2H), 4.44–4.51 (m, 2H), 5.26 (d, 2H), 5.39–5.69 (q, 2H), 7.30 (s, 1H), 7.67 (dd, 1H), 7.94 (d, 1H), 8.24 (d, 1H). [M + H]⁺ calculated for C₄₆H₆₄N₂O₁₉, 948.41; found, 949.13.

Results and discussions

Synthesis of self-assembling SN38 prodrugs

Fig. 1A and Scheme S1 (ESI[†]) show the molecular design of the studied self-assembling prodrugs (SAPDs), consisting of the hydrophobic SN38 and hydrophilic OEG₅-OH. The commercially available SN38 possesses two different hydroxyl groups located at positions 10 and 20, exhibiting varied reactivity when coupled with OEG₅-OH *via* carbonate bonds. By carefully regulating the molar ratio between SN38 and OEG₅-OH, only phenolic (C10) or both hydroxyl groups were conjugated, yielding mono- and di-functional SN38 (labeled as 10-OEG-SN38 and di-OEG-SN38), respectively. Furthermore, the phenolic hydroxyl group could be protected by *tert*-butyloxycarbonyl (Boc), and the residual C20-hydroxyl group was then capped by OEG₅-OH.

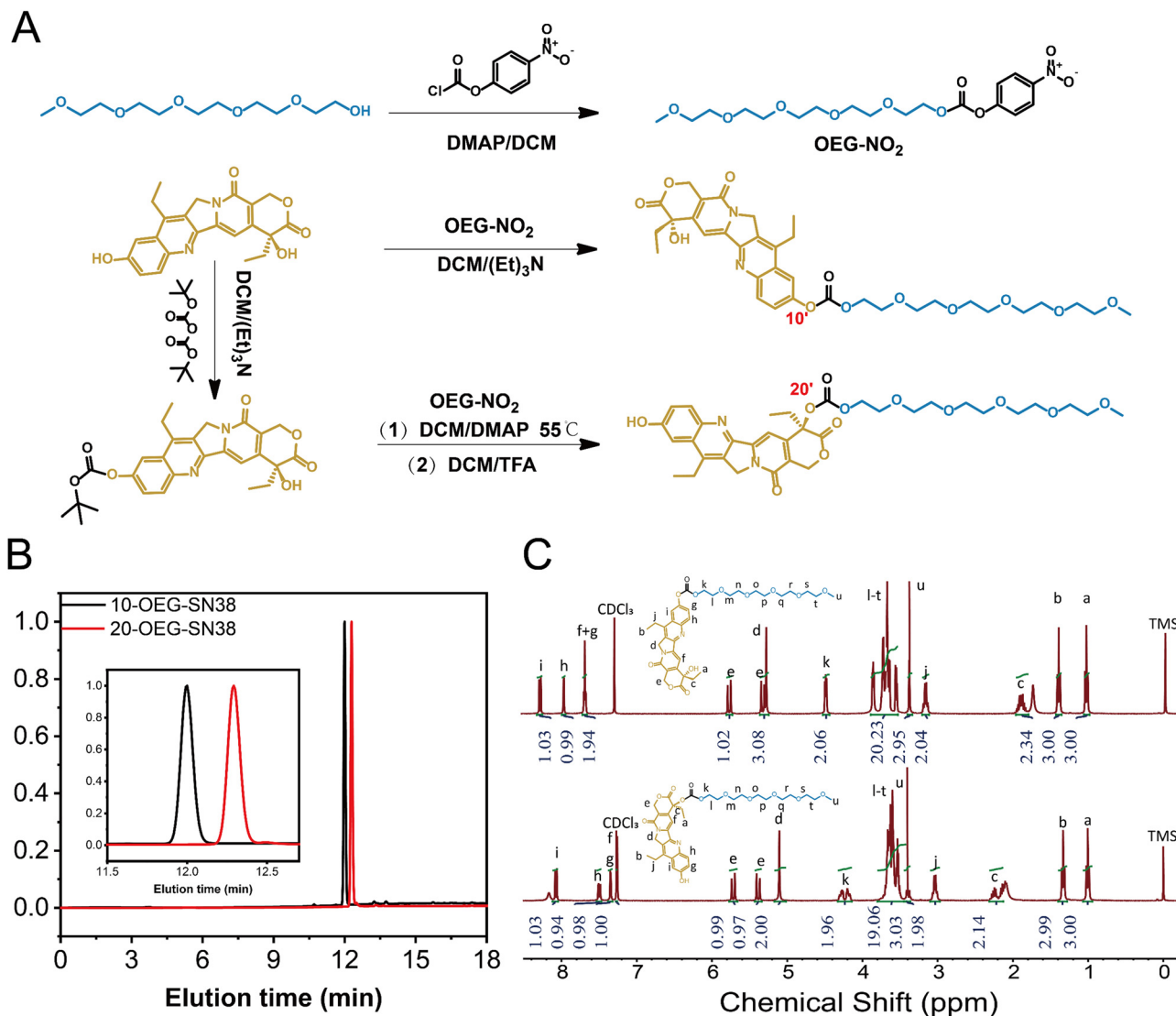


Fig. 1 Schematic illustration of the design and synthesis of SN38 SAPDs (A). Comparison of the RP-HPLC chromatograms of 10-OEG-SN38 and 20-OEG-SN38 (B) and comparison of ^1H NMR spectra of 10-OEG-SN38 and 20-OEG-SN38 (C).

Another mono-substituted prodrug (20-OEG-SN38) was obtained after deprotecting and served as the regio-isomer of 10-OEG-SN38. Details of the synthesis of these self-assembling prodrugs can be found in Section 1–4 and Fig. S1–S6 (ESI †).

The HPLC trace of each compound, as shown in Fig. 1B, displays a narrow and unimodal peak, confirming the high purity of the obtained molecules. The chemical accuracy of each sample was further confirmed by LC-MS, with a series of single m/z peaks in excellent accordance with the calculated values (Fig. S1–S6, ESI †). All these characterizations clearly demonstrate the successful synthesis of the prodrugs. The resultant prodrugs were purified using reversed-phase high-performance liquid chromatography (RP-HPLC), and their chemical structures and purity were fully characterized by nuclear magnetic resonance (NMR), analytical HPLC and liquid chromatography-mass spectrometry (LC-MS). The characteristic resonances of both precursory motifs (SN38 and OEG) could

be captured, and the integration agrees well with the proposed chemical structures.

Interestingly, the subtle variations between samples 10-OEG-SN38 and 20-OEG-SN38, a pair of regio-isomers with the same composition but different architectures, can be clearly identified by HPLC and ^1H NMR. The eluting time of sample 20-OEG-SN38 is substantially longer than that of 10-OEG-SN38, which can be well resolved due to the appreciable difference (Fig. 1B). This may indicate that sample 20-OEG-SN38 possesses a stronger hydrophobic interaction. As depicted in Fig. 1C, obvious disparities emerge within the 4–8 ppm range corresponding to various modifications at distinct positions of SN38. Specifically, the 20-OEG-SN38 spectrum exhibits noteworthy variations. The peaks corresponding to OEG proximal to carbonate bonds undergo fragmentation into multiple peaks, accompanied by chemical shift variations from 4.5 ppm to 4.2 ppm due to the influence of the chiral carbon. In contrast, both 10-OEG-SN38

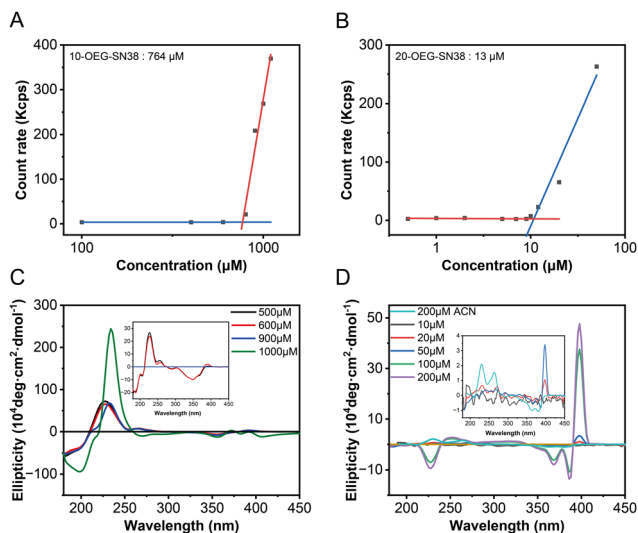


Fig. 3 Determination of self-assembly capacity and supramolecular stability. CMC was measured using DLS methods through the mutation of the count rate. 10-OEG-SN38 (A) and 20-OEG-SN38 (B). CD for various concentrations around CAC: 10-OEG-SN38 (C) and 20-OEG-SN38 (D).

nanofibers (Fig. 3C). Meanwhile, concentrations surpassing 900 μM yielded a notable positive peak at 240 nm, indicative of assembly formation for 10-OEG-SN38 (Fig. 3D). The estimated values are 900–1000 μM for 10-OEG-SN38 and 10–20 μM for 20-OEG-SN38. Both CMC and CAC values suggest that the self-assembly capability of 10-OEG-SN38 significantly decreases compared with that of 20-OEG-SN38, which may be due to the reduction of aromatic interactions resulting from the steric hindrance by the attached OEG on the benzene ring. These results indicate that various modification sites of SN38 significantly affect their associations and molecular arrangement, further affecting the assembly capability.

Drug release

To explore drug release properties, we performed degradation experiments at 37 $^{\circ}\text{C}$ in PBS solutions with a concentration of 200 μM . Because the solubility of SN38 is extremely poor, we chose to utilize the remaining ratio of SAPDs for detection by RP-HPLC. As shown in Fig. 4A, 20-OEG-SN38 exhibits a lower

degradation rate than that of 10-OEG-SN38, indicating a higher level of stability. Fig. 4B and C show a significant difference in the stability and degradation profiles between isomers at pH 7.4 monitored *via* analytical HPLC. Two peaks were observed in HPLC traces in the first hour, located at 8.5 min and 12 min, with the remaining ratio of 10-OEG-SN38 rapidly weakening to 40% (Fig. 4B). Monitored by LC-MS, the additional peak at 8.5 min was assigned to the carboxylate form of the prodrug (Scheme S2, ESI †) rather than the parent drug SN38 after carbonate cleavage. To confirm the pH-dependent hydrolysis of lactone, we investigated the stability of lactone in SN38 at pH 5.4. The corresponding peak is absent, revealing that the lactone stability of 10-OEG-SN38 is promoted at a lower pH value (Fig. S10, ESI †). Conversely, in the case of 20-OEG-SN38, the carboxylate form was not captured at both pH levels, which may be attributed to the enhanced stability of lactone by chemical modification at the 20-site.³⁹ It is well known that the release of the SN38 parent drug incorporates the disassembly of supramolecular structures and the subsequent hydrolysis of carbonate bonds. Here, benefiting from the lower CMC, 20-OEG-SN38 maintains a stable assembly status at a concentration of 200 μM , which can reduce solvent and ion contact and increase the stability of prodrugs. Our results reveal that the regio architecture can significantly influence the drug release process by altering chemical stability and self-assembly capability.

Cytotoxicity

We next studied the *in vitro* cytotoxicity against colorectal cancer cells CT26 and breast cancer cells MDA-MB-231 using SAPDs and the controls (*i.e.*, the parent drug SN38 and clinically used prodrug irinotecan) at various concentrations. The SAPDs were incubated with tumor cells for 48 hours, and their efficacy was evaluated by applying MTT methods *via* a dose-response relationship assay based on SN38 concentration (Fig. 5). Fig. 5A illustrates that the IC_{50} values of irinotecan, a clinical medication used for colorectal cancer, reach approximately 74 443 nM for CT26 cancer cells. Both SN38 SAPDs exhibit lower IC_{50} values with 518 nM for the 10-site and 1517 nM for the 20-site, suggesting a more effective inhibition of colorectal tumor cells in comparison to irinotecan. In contrast

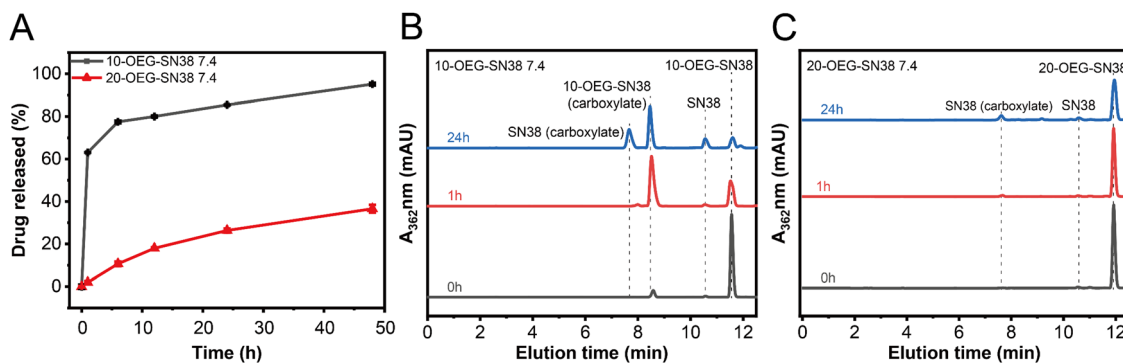


Fig. 4 Drug release of SN38 SAPDs at 200 μM in PBS at pH 7.4. Drug release plots of SAPDs (A) and comparison of HPLC spectra at different time points at pH 7.4: 10-OEG-SN38 (B) and 20-OEG-SN38 (C).

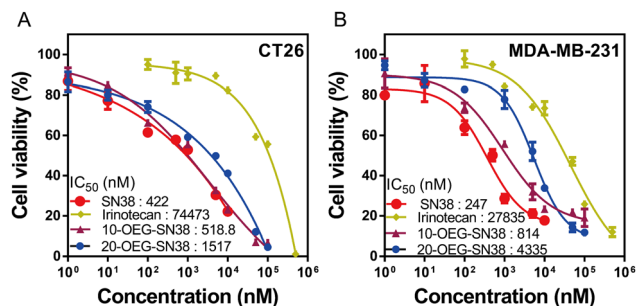


Fig. 5 *In vitro* cell cytotoxicity of 10/20-OEG-SN38 against CT-26 colorectal cancer cells (A) and MDA-MB-231 breast cancer cells (B), with both free SN38 and irinotecan as controls (48-h incubation).

to CT26 cells, both SAPDs exhibit a higher IC₅₀ in MDA-MB-231 cells. This lower toxicity may arise from the reduction of the degradation rate of carbonate bonds due to the relatively lower pH value within the microenvironment of breast cancer cells in comparison to colorectal cancer cells.⁴⁰ It is noteworthy that the efficacies of SAPDs are just slightly lower than those of the parent drug SN38, indicating that both SAPDs can effectively release the parent drug in the cellular environment. Moreover, there are still differences in efficacy between the isomers depending on their concentration levels.

At lower concentrations, 10-OEG-SN38 shows a higher level of cytotoxicity due to the faster hydrolysis of the carbonate bond with the phenolic hydroxyl group. Nevertheless, at concentrations ranging from 50 to 100 μ M, 20-OEG-SN38 exhibits a lower cell survival rate and shows a continuous decreasing trend, especially in MDA-MB-231 cells (Fig. 5B). As mentioned above, the lactone ring of SN38 was easily opened to reduce toxicity when modified on the 10-site but remained stable on the 20-site. As the concentration increases, 20-site may release more active ingredients compared to 10-site at the same concentration, resulting in a variety of toxicity between isomers. Moreover, above its CMC (13 μ M), the self-assembled nanostructures may play a certain role in cell internalization. Therefore, we can conclude that both SAPDs have excellent *in vitro* cytotoxicity, underscoring their substantial anticancer potential.

In vivo antitumor efficacy

To further understand how the regio architecture of SAPDs affects their *in vivo* performance, the antitumor efficacies of the regio-isomeric prodrugs were evaluated in a CT26 tumor model of BALB/c mice (see details in ESI†). The irinotecan dosage was set at 30 mg kg⁻¹ every two days near its maximum tolerated dosage.⁴¹ Similarly, the dosage of SN38 in our prodrugs was 34.3 mg kg⁻¹, matching the SN38 equivalent in irinotecan. When the tumor volume reached \sim 100 mm³ after tumor inoculation, the drugs were administered once every two days for six doses (*i.e.*, day 1, 3, 5, 7, 9, and 11) using physiological saline as a blank control. During the experiment, the weight and tumor volume of the mice were recorded as detection indicators of efficacy and safety. The body weights and tumor volumes of the mice are shown in Fig. 6A and B. After the fifth dose (day 9), the tumor volumes of the saline, irinotecan, 10-OEG-SN38, and 20-OEG-SN38 groups approached 586 mm³, 410 mm³, 124 mm³, and 98 mm³, respectively. Both SAPDs exhibited a more significant inhibitory effect on tumor growth compared with irinotecan, probably attributed to higher cytotoxicity and improved pharmacokinetics. Interestingly, although the group receiving 10-OEG-SN38 showed significant inhibition of tumor growth, we observed severe weight loss and even death in the studied animals within 11 days (Fig. 6A and C). This observation suggests that the 10-OEG-SN38 has severe toxicities in the animals studied. With a high CMC, 10-OEG-SN38 is rapidly diluted to small molecules in the bloodstream after injection, possibly leading to a fast drug release and causing toxicity to normal tissues. However, throughout the 20-OEG-SN38 treatment period, the average weight of the mice remained stable (Fig. 6A) and the 20-OEG-SN38 group showed the slowest tumor volume growth among all the treated groups (Fig. 6B). Additionally, the administration of 20-OEG-SN38 increased the median survival from 15 d (the control group) to 23 d, while the median survivals of the other groups were 11 d (10-OEG-SN38) and 17 d (irinotecan) (Fig. 6C). A reasonable explanation is that 20-OEG-SN38 can retain its nanostructure with low CMC (13 μ M) upon dilution in the circulation. This could prevent rapid renal clearance and prolong circulation to improve efficacy and safety. Our results revealed the differences in toxicity and efficacy of SN38 SAPDs when modified

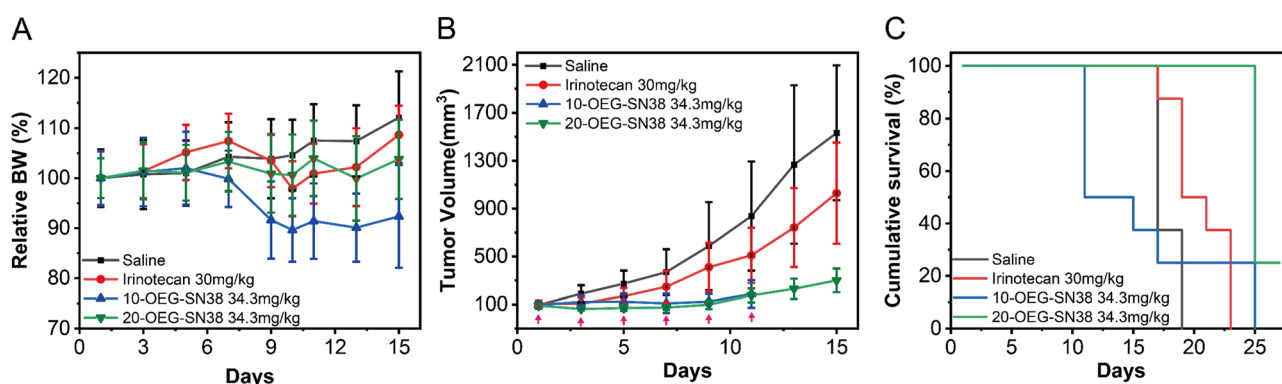


Fig. 6 *In vivo* antitumor efficacy of SAPDs using irinotecan and saline as the control group with 8 mice in each group. Relative body weight (A), tumor volume (B), and percent survival (C) plots of mice between isomers.

at 10-site and 20-site, establishing the correlations among molecular design, supramolecular stability, *in vitro* cytotoxicity and *in vivo* efficacy.

Conclusions

In this article, we synthesized a group of isomers *via* modification at different hydroxyl sites on SN38 to investigate their self-assembly behavior and biological functions. The SN38 SAPDs were self-assembled into giant nanotubes and nanofibers when OEG was anchored onto 10- or 20-positions. The SN38 SAPD with OEG at position 10 showed weaker aromatic associations and lower assembly capacity compared with SN-38 modified at position 20 due to the steric hindrance from OEG on the benzene ring that disrupted the close π - π stacking. The chemical and supramolecular stability of SAPDs can further influence the drug release, cytotoxicity, and therapeutic efficacy of the SAPDs both *in vitro* and *in vivo*. 20-OEG-SN38 exhibited lower cytotoxicity because of the slower hydrolysis of its carbonate bond; however, its therapeutic efficacy in tumor inhibition was better than that of commercial irinotecan. The 20-OEG-SN38 with a lower CMC retains its supramolecular integrity in the circulation, resulting in longer circulation and significantly retarding the growth of the tumor. Overall, our results indicate that the isomerization of SN38-OEG had significant effects on their associations, molecular arrangement in the assemblies, assembly capability, and, eventually, anticancer effects. Our work also presented a simplified design of amphiphilic prodrugs *via* direct OEGylation and gave an example of solely using the molecular interactions among drug units to create supramolecular drug assemblies without other directional intermolecular forces, such as hydrogen bonding. We hope that the current research can provide new insights into the selective modification of therapeutics into SAPDs and motivate the future design of simple SAPD systems.

Author contributions

Z. T. and H. S. designed research; Z. T., J. Z., W. L., and K. W. performed research; Z. T., D. Z., and H. S. analysed data; Z. G., D. Z., and H. S. supervised the project; Z. T., D. Z., and H. S. wrote and revised the paper.

Conflicts of interest

There are no conflicts to declare.

Acknowledgements

This work was supported by the National Natural Science Foundation of China (52273136 to H.S.), the Sichuan Science and Technology Program (2023YFH0071 to H.S., 2023NSFS C0306 to D.Z.) and the Opening Project of State Key Laboratory of Polymer Materials Engineering (Sichuan University) (Grant No. sklpm2022-3-14 to H.S.). This work was also financially

supported by Med-X Innovation Program of Med-X Center for Materials, Sichuan University (MCM202304 to H.S.) and the Fundamental Research Funds for the Central Universities (YJ202210 to H.S.). We would be also grateful to Minghua Zhang of the College of Polymer Science and Engineering at Sichuan University for his help of TEM analysis.

Notes and references

- H. Acar, S. Srivastava, E. J. Chung, M. R. Schnorenberg, J. C. Barrett, J. L. LaBelle and M. Tirrell, Self-Assembling Peptide-Based Building Blocks in Medical Applications, *Adv. Drug Delivery Rev.*, 2017, **110–111**, 65–79.
- M. J. Webber, E. A. Appel, E. W. Meijer and R. Langer, Supramolecular Biomaterials, *Nat. Mater.*, 2016, **15**(1), 13–26.
- T. Aida, E. W. Meijer and S. I. Stupp, Functional Supramolecular Polymers, *Science*, 2012, **335**(6070), 813–817.
- P. W. J. M. Frederix, G. G. Scott, Y. M. Abul-Haija, D. Kalafatovic, C. G. Pappas, N. Javid, N. T. Hunt, R. V. Ulijn and T. Tuttle, Exploring the Sequence Space for (Tri-)Peptide Self-Assembly to Design and Discover New Hydrogels, *Nat. Chem.*, 2015, **7**(1), 30–37.
- Y. Zhang, T. Zhou, Y. Qi, Y. Li, Y. Zhang, Y. Zhao, H. Han and Y. Wang, Engineered Assemblies from Isomeric Pentapeptides Augment Dry Eye Treatment, *J. Controlled Release*, 2024, **365**, 521–529.
- Y. Wang, Y. Lyu and Z. Li, Constitutionally Isomeric Peptides: Subtle Changes Leading to Dramatic Differences in Properties, *ACS Appl. Eng. Mater.*, 2024, DOI: [10.1021/acsaem.3c00787](https://doi.org/10.1021/acsaem.3c00787).
- H. Cui, A. G. Cheetham, E. T. Pashuck and S. I. Stupp, Amino Acid Sequence in Constitutionally Isomeric Tetrapeptide Amphiphiles Dictates Architecture of One-Dimensional Nanostructures, *J. Am. Chem. Soc.*, 2014, **136**(35), 12461–12468.
- A. Lampel, S. A. McPhee, H.-A. Park, G. G. Scott, S. Humagain, D. R. Hekstra, B. Yoo, P. W. J. M. Frederix, T.-D. Li, R. R. Abzalimov, S. G. Greenbaum, T. Tuttle, C. Hu, C. J. Bettinger and R. V. Ulijn, Polymeric Peptide Pigments with Sequence-Encoded Properties, *Science*, 2017, **356**(6342), 1064–1068.
- Y. Wang, K. Kaur, S. J. Scannelli, R. Bitton and J. B. Matson, Self-Assembled Nanostructures Regulate H₂S Release from Constitutionally Isomeric Peptides, *J. Am. Chem. Soc.*, 2018, **140**(44), 14945–14951.
- Z. Liu, J. Guo, Y. Qiao and B. Xu, Enzyme-Instructed Intracellular Peptide Assemblies, *Acc. Chem. Res.*, 2023, **56**(21), 3076–3088.
- M. Yi, Z. Feng, H. He, D. Dinulescu and B. Xu, Evaluating Alkaline Phosphatase-Instructed Self-Assembly of d-Peptides for Selectively Inhibiting Ovarian Cancer Cells, *J. Med. Chem.*, 2023, **66**(14), 10027–10035.
- S. I. S. Hendrikse, L. Su, T. P. Hogervorst, R. P. M. Lafleur, X. Lou, G. A. van der Marel, J. D. C. Codee and E. W. Meijer, Elucidating the Ordering in Self-Assembled Glycocalyx Mimicking Supramolecular Copolymers in Water, *J. Am. Chem. Soc.*, 2019, **141**(35), 13877–13886.

- 13 H. Su, W. Zhang, H. Wang, F. Wang and H. Cui, Paclitaxel-Promoted Supramolecular Polymerization of Peptide Conjugates, *J. Am. Chem. Soc.*, 2019, **141**(30), 11997–12004.
- 14 A. G. Cheetham, R. W. Chakraborty, W. Ma and H. Cui, Self-Assembling Prodrugs, *Chem. Soc. Rev.*, 2017, **46**(21), 6638–6663.
- 15 H. Su, J. M. Koo and H. Cui, One-Component Nanomedicine, *J. Controlled Release*, 2015, **219**, 383–395.
- 16 H. Ren, X.-Z. Zeng, X.-X. Zhao, D. Hou, H. Yao, M. Yaseen, L. Zhao, W. Xu, H. Wang and L.-L. Li, A Bioactivated in Vivo Assembly Nanotechnology Fabricated NIR Probe for Small Pancreatic Tumor Intraoperative Imaging, *Nat. Commun.*, 2022, **13**(1), 418.
- 17 C. H. Liang, Y. X. Chen, D. B. Zheng, T. Y. Xu, G. J. Pu, Y. M. Chen, L. Wang, Z. M. Yang and H. M. Wang, Pathway-Dependent Supramolecular Polymerization of Camptothecin Derivatives into Filaments for Chemotherapy and Imaging, *Appl. Mater. Today*, 2020, **20**, 100787.
- 18 K. Kataoka, A. Harada and Y. Nagasaki, Block Copolymer Micelles for Drug Delivery: Design, Characterization and Biological Significance, *Adv. Drug Delivery Rev.*, 2012, **64**, 37–48.
- 19 J. Bhattacharyya, J. J. Bellucci, I. Weitzhandler, J. R. McDaniel, I. Spasojevic, X. Li, C.-C. Lin, J.-T. A. Chi and A. Chilkoti, A Paclitaxel-Loaded Recombinant Polypeptide Nanoparticle Outperforms Abraxane in Multiple Murine Cancer Models, *Nat. Commun.*, 2015, **6**(1), 7939.
- 20 H. Ren, X.-Z. Zeng, X.-X. Zhao, D. Hou, H. Yao, M. Yaseen, L. Zhao, W. Xu, H. Wang and L.-L. Li, A Bioactivated in Vivo Assembly Nanotechnology Fabricated NIR Probe for Small Pancreatic Tumor Intraoperative Imaging, *Nat. Commun.*, 2022, **13**(1), 418.
- 21 Y. Fang and H. Wang, Molecular Engineering of Peptide–Drug Conjugates for Therapeutics, *Pharmaceutics*, 2022, **14**(1), 212.
- 22 Y. Pommier, Topoisomerase I Inhibitors: Camptothecins and Beyond, *Nat. Rev. Cancer*, 2006, **6**(10), 789–802.
- 23 A. Makimoto, H. Mugishima, T. Taga, Y. Ishida, Y. Nagatoshi, K. Ida, M. Kumagai, T. Kimura, Y. Ohashi and M. Kaneko, Registration-Directed Phase 1/2 Trial of Irinotecan for Pediatric Solid Tumors, *Pediatr. Int.*, 2019, **61**(5), 453–458.
- 24 R. H. J. Mathijssen, R. J. van Alphen, J. Verweij, W. J. Loos, K. Nooter, G. Stoter and A. Sparreboom, Clinical Pharmacokinetics and Metabolism of Irinotecan (CPT-11), *Clin. Cancer Res.*, 2001, **7**(8), 2182–2194.
- 25 C. Bailly, Irinotecan: 25 Years of Cancer Treatment, *Pharmacol. Res.*, 2019, **148**, 104398.
- 26 Y. Huang, L. Wang, Z. Cheng, B. Yang, J. Yu, Y. Chen and W. Lu, SN38-Based Albumin-Binding Prodrug for Efficient Targeted Cancer Chemotherapy, *J. Controlled Release*, 2021, **339**, 297–306.
- 27 J. Zhao, S. Ma, Y. Xu, X. Si, H. Yao, Z. Huang, Y. Zhang, H. Yu, Z. Tang, W. Song and X. Chen, *In Situ* Activation of STING Pathway with Polymeric SN38 for Cancer Chemotherapy, *Biomaterials*, 2021, **268**, 120542.
- 28 Y. Zheng, X. Yan, Y. Wang, X. Duan, X. Wang, C. Chen, D. Tian, Z. Luo, Z. Zhang and Y. Zeng, Hydrophobized SN38 to Redox-Hypersensitive Nanorods for Cancer Therapy, *J. Mater. Chem. B*, 2019, **7**(2), 265–276.
- 29 Y. Liu, H. Piao, Y. Gao, C. Xu, Y. Tian, L. Wang, J. Liu, B. Tang, M. Zou and G. Cheng, Comparison of Two Self-Assembled Macromolecular Prodrug Micelles with Different Conjugate Positions of SN38 for Enhancing Antitumor Activity, *Int. J. Nanomed.*, 2015, **10**, 2295–2311.
- 30 X. Yang, H. Lu, Y. Tao, L. Zhou and H. Wang, Spatiotemporal Control over Chemical Assembly in Living Cells by Integration of Acid-Catalyzed Hydrolysis and Enzymatic Reactions, *Angew. Chem., Int. Ed.*, 2021, **60**(44), 23797–23804.
- 31 H. Wang, H. Su, T. Xu and H. Cui, Utilizing the Hofmeister Effect to Induce Hydrogelation of Nonionic Supramolecular Polymers into a Therapeutic Depot, *Angew. Chem., Int. Ed.*, 2023, **62**(43), e202306652.
- 32 Y. Cai, H. Shen, J. Zhan, M. Lin, L. Dai, C. Ren, Y. Shi, J. Liu, J. Gao and Z. Yang, Supramolecular “Trojan Horse” for Nuclear Delivery of Dual Anticancer Drugs, *J. Am. Chem. Soc.*, 2017, **139**(8), 2876–2879.
- 33 Y. Cai, B. Zhu, X. Shan, L. Zhou, X. Sun, A. Xia, B. Wu, Y. Yu, H. H. Zhu, P. Zhang and Y. Li, Inhibiting Endothelial Cell-Mediated T Lymphocyte Apoptosis with Integrin-Targeting Peptide–Drug Conjugate Filaments for Chemoimmunotherapy of Triple-Negative Breast Cancer, *Adv. Mater.*, 2024, **36**(3), 2306676.
- 34 S. Zeng, H. Ou, Z. Gao, J. Zhang, C. Li, Q. Liu and D. Ding, HCPT-Peptide Prodrug with Tumor Microenvironment-Responsive Morphology Transformable Characteristic for Boosted Bladder Tumor Chemotherapy, *J. Controlled Release*, 2021, **330**, 715–725.
- 35 H. Su, F. Wang, W. Ran, W. Zhang, W. Dai, H. Wang, C. F. Anderson, Z. Wang, C. Zheng, P. Zhang, Y. Li and H. Cui, The Role of Critical Micellization Concentration in Efficacy and Toxicity of Supramolecular Polymers, *Proc. Natl. Acad. Sci. U. S. A.*, 2020, **117**(9), 4518–4526.
- 36 A. G. Cheetham, P. Zhang, Y. Lin, L. L. Lock and H. Cui, Supramolecular Nanostructures Formed by Anticancer Drug Assembly, *J. Am. Chem. Soc.*, 2013, **135**(8), 2907–2910.
- 37 H. Su, P. Zhang, A. G. Cheetham, J. M. Koo, R. Lin, A. Masood, P. Schiapparelli, A. Quiñones-Hinojosa and H. Cui, Supramolecular Crafting of Self-Assembling Camptothecin Prodrugs with Enhanced Efficacy against Primary Cancer Cells, *Theranostics*, 2016, **6**(7), 1065–1074.
- 38 A. G. Cheetham, P. Zhang, Y. Lin, L. L. Lock and H. Cui, Supramolecular Nanostructures Formed by Anticancer Drug Assembly, *J. Am. Chem. Soc.*, 2013, **135**(8), 2907–2910.
- 39 X. He, W. Lu, X. Jiang, J. Cai, X. Zhang and J. Ding, Synthesis and Biological Evaluation of Bis and Monocarbonate Prodrugs of 10-Hydroxycamptothecins, *Bioorg. Med. Chem.*, 2004, **12**(15), 4003–4008.
- 40 T. Volk, E. Jähde, H. P. Fortmeyer, K.-H. Glüsenkamp and M. F. Rajewsky, pH in Human Tumour Xenografts: Effect of Intravenous Administration of Glucose, *Br. J. Cancer*, 1993, **68**(3), 492–500.
- 41 T. Schluep, J. Cheng, K. T. Khin and M. E. Davis, Pharmacokinetics and Biodistribution of the Camptothecin–Polymer Conjugate IT-101 in Rats and Tumor-Bearing Mice, *Cancer Chemother. Pharmacol.*, 2006, **57**(5), 654–662.